Type of contribution:
Editorial
▶ Research Paper
Case Study
Review Paper
Scientific Data
Report of Tech. Application

mesi
e-issn. 2798-5245

Mechanical Engineering for Society and Industry
Vol. 5, No. 1 (2025) pp 245-256
https://doi.org/10.31603/mesi.13018

Investigation of discrepancies in isotropic material and structural properties in lattice frameworks

Ahmad Anas Arifin[1], I Made Londen Batan[1*], Michele Bici[2], Arif Wahjudi[1], Agus Sigit Pramono[1]

[1] Department of Mechanical Engineering, Institut Teknologi Sepuluh Nopember, Surabaya 60111, **Indonesia**
[2] Department of Mechanical and Aerospace Engineering, Sapienza University of Rome, Rome 00184, **Italy**
✉ londbatan@me.its.ac.id

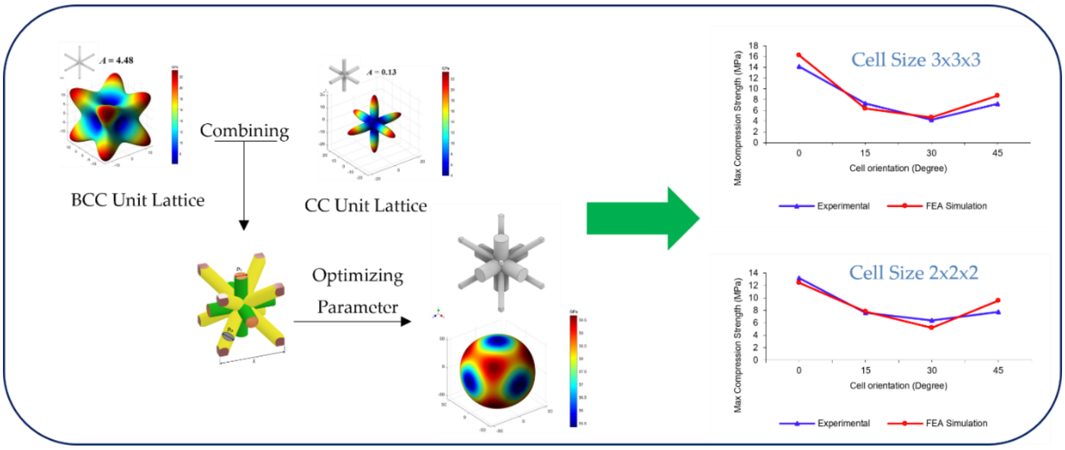

Highlights:

- The CC-BCC lattice showed near-isotropic material behavior at a CC/BCC strut diameter ratio of 2.5 (Zener index = 1.08).
- Finite element and compressive tests assessed isotropy of the CC-BCC lattice across different cell orientations and sizes.
- Tests confirmed that isotropy at the material level doesn't guarantee isotropy at the structural level due to orientation effects on strength.
- Smaller cell sizes achieved higher compressive strength than larger ones in both 0° and 45° orientations.
- This study highlights the importance of a multidisciplinary approach in designing and optimizing additively manufactured lattices.

Article info

Submitted:
2025-01-15

Revised:
2025-05-31

Accepted:
2025-06-04

This work is licensed under a Creative Commons Attribution-NonCommercial 4.0 International License

Publisher

Universitas Muhammadiyah Magelang

Abstract

Lattice structures have developed as a vital component in advanced engineering applications due to their superior strength-to-weight ratios and adjustable mechanical properties. This paper focuses on examining the correlation between the isotropic features of lattices at the material level and their structural performance. The research used near-isotropic Crossing-cylinder (CC)- Body Centered Cubic (BCC) cells in various orientations and sizes. Both experimental analysis and finite element analysis were used to examine the compressive strength of the structure in each orientation. The results reveal that cell orientation is important for determining failure modes and mechanical performance at the structural level. At 0°, the lattice has higher compressive strength and energy absorption due to effective load transfer via CC-aligned struts. In contrast, higher orientations (e.g., 15°, 30°, and 45°) are dominated by collapse-type failures, indicating anisotropic behavior in an otherwise isotropic design. Smaller cell sizes have more strength at lower orientations due to their higher relative density, but larger cells perform better at higher orientations.

Keywords: Lattice structures; Isotropic; Compressive strength; Failure modes

1. Introduction

There are several ways to increase an additively created structure's load-bearing capacity, such as altering the material or the production process. None of these, however, come without a hefty price tag. A lattice structure is more effectively designed to improve the load-bearing and energy-absorbing capacities of additively built components. Nevertheless, this calls for a multidisciplinary strategy in order to contribute for more sustainable environment [1]. Typically, a basic lattice unit repeated in two or three dimensions yields a lattice, a sort of porous structure. Lattice has many benefits, including heat management, energy absorption, acoustic vibrational dampening, and high strength-to-weight ratios [2]. Because of these exceptional qualities, lattice structures have revolutionized a wide range of industries, including energy absorbers and orthopaedic implants [3].

Lattice structures are classified into several categories based on the unit cell and the replication pattern used for cell construction. According to the unit cell, lattices can be divided into strut-based and surface-based types [4]. In terms of the replication pattern, there are three types: regular, pseudo-regular, and stochastic [5]. The use of lattice is very broad and specific to the conditions that one wants to achieve. The advantage of strut-based lattice cells is their flexibility to optimize the strength by using the ratio of the cross-sectional circular radius (r) to the edge length (s) [6]. By changing the ratio, it will also affect the relative density of the lattice cell that important in lattice structure. The higher the relative density, the greater the compressive strength of the lattice structure [7].

The commonly used technique to directionally controlled mechanical properties is the anisotropic strategy [8],[9]. However, designing near-isotropic lattices is also necessary for applications that require isotropy, where the force conditions come from all directions with equal magnitude [10]. It can also be implemented to ensure that the lattice is resilient and can sustain forces from all directions in cases where the force's direction is indeterminate. In order to assess whether lattice cell is materially isotropic or not, it is common to use Zener anisotropic index [11],[12]. It can be calculated by employing the numerical homogenization technique to derive an effective stiffness matrix [13]. The structure can be classified as isotropic if the Zener index A approaches 1. Although this strategy must be further investigated structurally [14].

One of the methods for controlling the anisotropic properties of a lattice involves combining several forms of basic lattices. The Face Centered Cubic (FCC) – Body Centered Cubic (BCC) forms can be combined and then parametrically optimized for the radius of the BCC lattice struts and the radius of the FCC lattice struts. A BCC radius/FCC radius ratio of 0.52 can be used to attain the isotropic condition [15]. Subsequently, the cross-fructum shape and the octet truss shape are combined to attain isotropic conditions. The cross-fructum is cylindrical in shape and has a tapered profile, which results in varying radii at both extremities. This is then used as a parameter for optimization to achieve isotropic conditions. The condition can be achieved with a ratio of the radius of the larger circle to the radius of the smaller circle at both ends of the cross-fructum of 1.25 [16].

Prior studies have combined two fundamental lattice types, such as Octet and Cross-fructum or FCC and BCC, in an effort to improve the isotropic nature of lattices. Even though body-centered cubic (BCC) and Crossing Cylinder (CC) are popular and frequently utilized lattice forms, no research has yet examined the combination of two lattice cells. The problem with earlier attempts to improve isotropic quality was that they mostly concentrated on the material level, proving isotropy solely in terms of material attributes. Unfortunately, studies about translating material isotropy into structural isotropy have not many discussed yet. It is essential to consider that a lattice that is materially isotropic may not be structurally isotropic. For example, the implementation of lattice structure in prosthetic legs with isotropic strategy lattice structure. If the optimization only to find materially isotropic lattice cell with A = 1. It may not be structurally isotropic, if we implement it directly to structure of the legs with specific configuration and orientation of lattice cell.

Therefore, this research aims to examine the correlation between the isotropic features of lattices at the material level and their structural performance. This study combines CC and BCC lattices to generate a novel near materially isotropic lattice structure. The compressive strength of the CC-BCC lattice will next be assessed experimentally and through simulations using Finite Element Analysis in a range of cell sizes and orientations.

2. Methods

2.1. Lattice Cell Design

The process of designing lattice cells using numerical solution method presented by Xie *et al*. [15] , a specific strain component is assigned a value of 1 during each step, while the remaining five components are set to zero in Eq. (1). Through this iterative process, the individual C values can be obtained separately.

$$Input: \begin{Bmatrix} \varepsilon_{11} \\ \varepsilon_{22} \\ \varepsilon_{33} \\ \varepsilon_{12} \\ \varepsilon_{13} \\ \varepsilon_{23} \end{Bmatrix} = \begin{Bmatrix} 1 \\ 0 \\ 0 \\ 0 \\ 0 \\ 0 \end{Bmatrix} \quad output: \begin{Bmatrix} \sigma_{11} \\ \sigma_{22} \\ \sigma_{33} \\ \sigma_{12} \\ \sigma_{13} \\ \sigma_{23} \end{Bmatrix} = \begin{Bmatrix} C_n \\ C_{ns} \\ C_{ns} \\ 0 \\ 0 \\ 0 \end{Bmatrix} \tag{1}$$

The boundary conditions for the normal strain $\varepsilon_{11} = 1$ specify that at $y = l_y$ the change in length Δl_y is equal to $0.001 l_y$, while zero displacement is maintained at the boundaries $y = 0, x = 0\,, x = l_x\,, z = 0, and\ z = l_z$. Additionally, at $y = l_y$, the change in length Δl_x is set to $0.0005 l_y$ and Δl_y is defined as $0.0005 l_x$ for varying x.

The stiffness tensor C can be estimated from the volume average value of the total stress [16]. The calculation formula is:

$$C_{ij} = \bar{\sigma} = \frac{1}{V}\int_V \sigma_{ij}(x, y, z)dV \tag{2}$$

The elastic modulus can be obtained as:

$$E = \frac{C_{11}^3 + 2C_{12}^3 - 3C_{11}C_{12}^2}{C_{11}^2 - C_{12}^2} \tag{3}$$

And the Zener anisotropy index A can be acquired as:

$$A = \frac{2C_{44}}{C_{11} - C_{12}} \tag{4}$$

The stiffness matrix can be derived by implementing the code developed by Dong *et al*. [17] in MATLAB to compute the analytical outcomes. Then, by combining the BCC lattice model with a strut diameter of a and the CC lattice model with a strut diameter of 2.5a, a lattice cell with near-isotropic properties was obtained, with a Zener index A = 1.08. The results of the lattice cell design evolution can be seen in **Figure 1**.

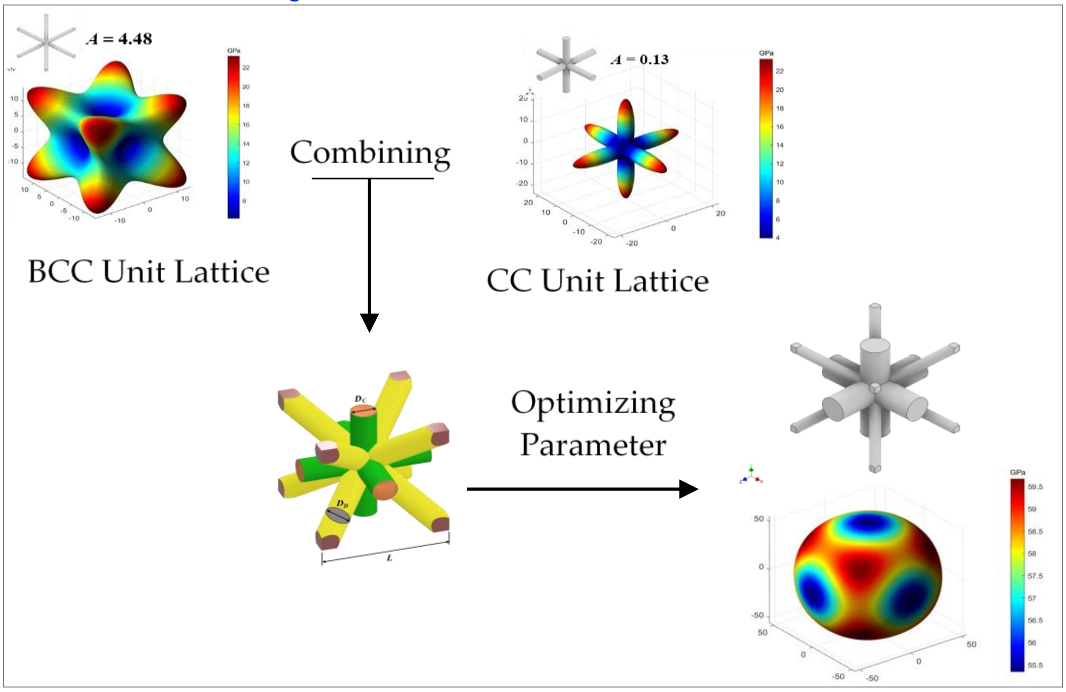

Figure 1. Design evolution of the lattice cell CC-BCC.[18]

The relative density of the lattice cell can be calculated using the Eq. (5), where V_L is the volume of the lattice cell and V_s is the volume of the solid cube. Thus, the relative density value for the optimized CC-BCC cell type is obtained as 16% (single cell). The advantage of this type of lattice is the flexibility to adjust materially isotropic level of lattice cell due to double parametric inputs (diameter of CC and diameter of BCC Lattice). It may not be achieved by previous lattice BCC and CC which only has single parametric input. The other advantage of CC-BCC cell is flexibility to adjust relative density in order to enhance strength in various direction.

$$\Phi = \frac{V_L}{V_s} \tag{5}$$

2.2. Additive Manufacturing

The author employs the additive manufacturing (AM) technology in this investigation. The initial category is fused deposition modeling (FDM). The FDM machine utilized in this research is the Flashforge Creator Pro 2 manufactured by Zhejiang Flashforge 3D Technology Co., LTD. It operates with 1.75 mm PLA Filament from the eSun brand. The PLA material has a density of 1.2 g/cm³, Young's modulus of 3500 MPa, yield tensile stress of 63.2 MPa, ultimate tensile strength of 65 MPa, and a Poisson's ratio of 0.36. The slicing procedure is performed using Flashprint 5 © software, which is the proprietary software developed by the Flashforge brand. The 3D printing parameters have been set as follows: the print nozzle diameter is 0.4 mm, the nozzle temperature has been maintained at 210 °C with 5°C tolerance, the bed temperature has been maintained at 40 °C, the layer height has been established at 0.18 mm, the print infill has been configured to 100%, and the print speed has been set to 60 mm/min.

2.3. Specimen and Compression Testing

The specimen manufacturing process in this study uses the FDM process. The results of the specimens can be seen in **Figure 2**. Eight specimens are chosen due to 4 levels of orientation and 2 levels of cell size. The orientations were 0 , 15, 30, 45 deg, and size cell are 8 mm and 12 mm with cube size of 24 x 24 x 24 mm. therefore, number of cell are 2 x 2 x 2 and 3 x 3 x 3. The variation of orientations was used to investigate the isotropic properties of lattice structure. Normally, Isotropic lattices have same mechanical properties in all direction. The Uniaxial Compression Test was conducted on all specimens using the Universal Testing Machine WDW-20E from Time Group Inc with a 20kN load cell. The applied compression speed in this study is 0.5 mm/min with a final deformation of 40% h0. The direction of pressure applied is perpendicular to the printing direction. The result obtained from this compression test is data on Load vs displacement. Then, the method for analyzing damage and failure is carried out through visual inspection. The obtained data is then processed into stress-strain graphs and energy absorption ability using the Eqs. (6) to (9) [19].

$$\sigma_{N,c} = \frac{P_c}{A_{0,eq}} \tag{6}$$

$$\mathrm{A}_{0,eq} = \frac{V_L}{h_0} = (1-\phi){h_0}^2 \tag{7}$$

$$\varepsilon_{N,c} = \frac{u_c}{h_0} \tag{8}$$

$$\mathrm{W}_c = \int_{\varepsilon=0}^{\varepsilon=0.4} \sigma_{N,c}\varepsilon_{N,c}\, d\varepsilon \tag{9}$$

Where:
$\sigma_{N,c}$: Nominal Compressive Stress (MPa)
$\varepsilon_{N,c}$: Nominal Compressive Strain (%)
P_c : Compressive Load (N)
$\mathrm{A}_{0,eq}$: Equivalent Cross Section Area of Cell (mm^2)
u_c : Compressive displacement (mm)
h_0 : Initial height (mm)
W_c : Energy absorption per unit volume calculated up to ε = 0.4.

The value of ε=0.4 is chosen because the graph that appears after that, starts to become unstable. The calculated values of A0, eq and φ can be seen in **Table 1**.

Table 1. Equivalent cross section area of cell and density on CC-BCC lattice

Number of Specimen	Orientation (Deg)	Cell Size (mm)	Number of Cell	Size h_0 (mm)	Volume Lattice VL (mm^3)	Volume Solid Cube vs (mm^3)	Density Φ (%)	Eq. Cross Section Area of Cell (mm^2)
1	0	08:08:08	03:03:03	24	3345.45	13824	0.24	139.39
2	0	12:12:12	02:02:02	24	2981.73	13824	0.22	124.24
3	15	08:08:08	03:03:03	24	3343.4	13824	0.24	139.31
4	15	12:12:12	02:02:02	24	3088.13	13824	0.22	128.67
5	30	08:08:08	03:03:03	24	3196.67	13824	0.23	133.19
6	30	12:12:12	02:02:02	24	3350.13	13824	0.24	139.59
7	45	08:08:08	03:03:03	24	3263.37	13824	0.24	135.97
8	45	12:12:12	02:02:02	24	3518.18	13824	0.25	146.59

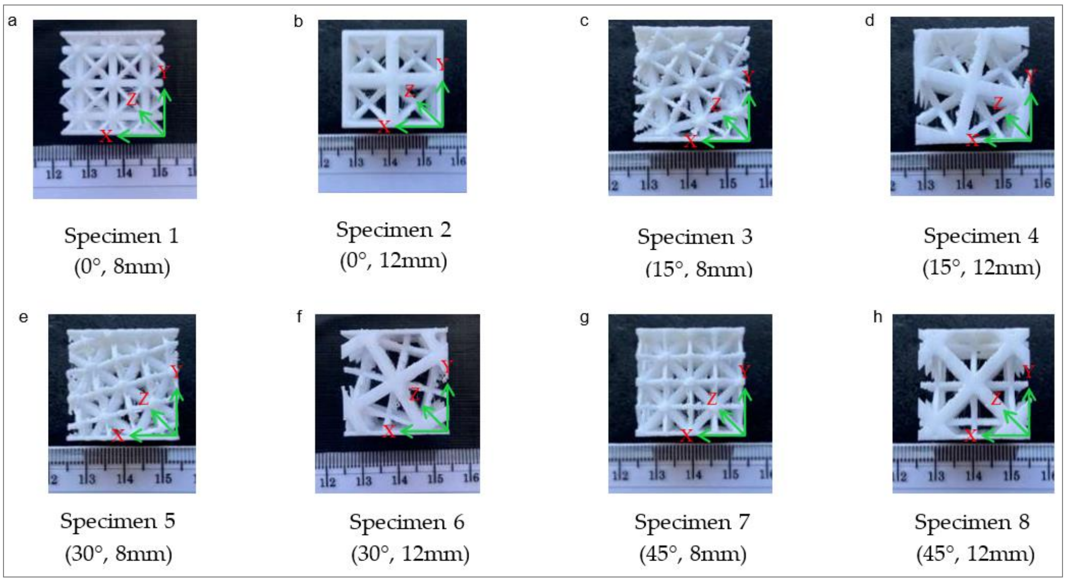

Figure 2. Specimen Fabrication using FDM. The images a-h are Specimen 1-8 Lattice CC-BCC according to Table 1

2.4. Finite Element Analysis

The finite element analysis (FEA) method is used in the numerical simulation used in this investigation. The simulation used a mesh size of 0.4 mm with element type tetrahedrons. The respective size and type are chosen based on the topology of the lattice, which is complex. Additionally, a convergence level for the von Mises stress is kept below 10% to guarantee the accuracy of the simulation findings [20]. The maximum load that the specimen can support is then determined using the Eq. (10) and the von Mises stress data that was obtained.

$$F_{max} = \frac{\sigma_{UTS}\ x\ F_{in}}{\sigma_{FEA}} \tag{10}$$

Where:

F_{max} : Maximum bearable load of the specimen (N)
σ_{UTS} : Ultimate tensile strength (65 MPa)
σ_{FEA} : Von misses Stress from FEA Simulation (MPa)
F_{in} : Input force (100 N)

3. Results and Discussion

3.1. Failure Mode of Lattice Structure

In general, lattice structures have three types of deformation modes [21]. The first deformation is buckling. Buckling occurs in structures or struts that have an axis orientation that is quasi-collinear with the direction of the normal or the direction of the applied force. Bending is the second form of deformation. Bending occurs in constructions or struts that have an axis orientation that is nearly perpendicular to the direction of the normal or the direction of the applied force [22]. The third deformation is characterized by the collapse of the object. Collapse is the result of a structure undergoing brittle deformation. This suggests that the force applied has surpassed the maximum capacity of the structure to endure it.

Based on the failure modes observed in **Figure 3**, a pattern can be seen that as the cell orientation increases, the failure mode is dominated by the collapse type. In contrast, at a cell orientation of 0°, both buckling and bending failure modes are still present, while at a cell orientation of 45°, no buckling or bending failure modes are found at all. This indicates that the compressive strength of specimens with a cell orientation of 45° is lower than that of specimens with a cell orientation of 0°.

In specimens 1-8, a diagonal shear mechanism failure was found with double shear bands at 45° towards the direction of the applied force until reaching layer crushing. The form of failure mode like this has the same trend as previous research by A. Kumar *et al.* [19]. It should also be noted that the size of the cell also affects the mode of failure that occurs. Smaller cell sizes tend to be more prone to collapse compared to specimens with larger cell sizes [23]. This happens because the diameter of the strut plays a significant role in resisting the forces that occur. A larger diameter strut will more easily create buckling and/or bending failure modes before collapse occurs [24]. The size and orientation of cells are interconnected with each other to create the mode of failure that occurs. In the following discussion, we will explore how this mode of failure affects the amount of compressive energy that can be absorbed by the lattice structure.

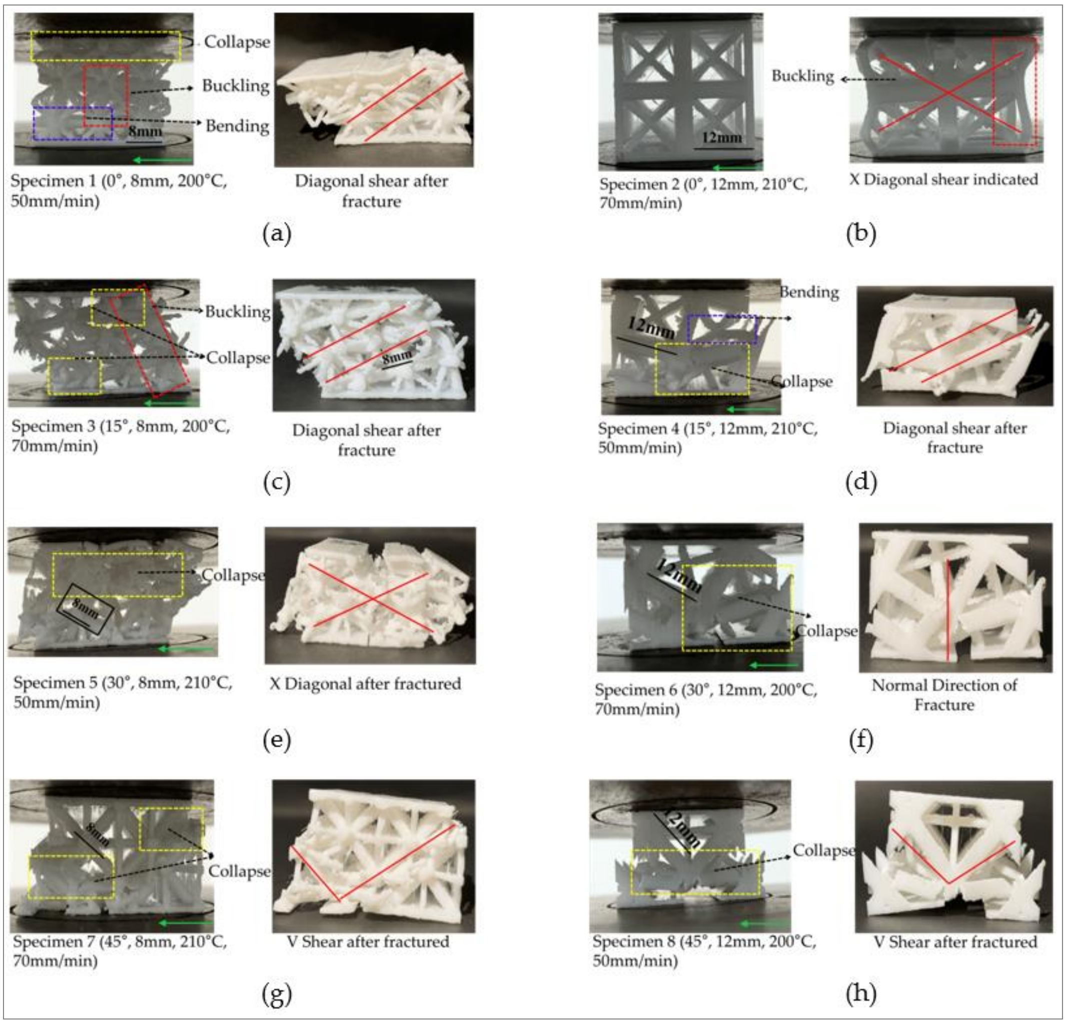

Figure 3. Experimental compressive deformation of CC-BCC Orientation 0°-45°. (a,c,e,g) cell size 8mm and (b,d,f,h) cell size 12mm. The green arrow indicates the build direction

3.2. Load Deformation Result

The study employed the uniaxial compression test for compression testing. **Figure 4** displays the outcomes of the uniaxial compression test. This investigation has identified three locations of deformation [19],[21],[25]. 1) The almost straight elastic region, indicated by a red circle; 2) The plateau region, where the structure starts to collapse, indicated by a yellow circle; 3) The densification region, where the stress response increases rapidly, indicated by a green circle. All compression responses obtained from the uniaxial compression tests of the three types of lattices are analyzed using a general analysis for polymeric lattice structures and foams.

The compression response begins in the linear elastic region. The linear elastic region has a slope of the line or gradient that represents the characteristic elastic modulus (N/mm^2) of the structure. After exceeding the elastic limit, the lattice structure begins to exhibit phenomena in the form of permanent plastic deformation [26]. This occurs as a result of the buckling, bending, and collapse deformation modes that have been discussed in the previous subsection. The area between the elastic limit and the yellow point with the number 2 is referred to as the plateau region. The plateau region is marked by a sharp decline in stress levels. Almost all lattices have recovery strength to withstand loads again. Recovery strength is indicated by the rise of the stress graph. This is indicated at the green point number 3. Densification occurs when the forces transferred within the body lattice begin to stabilize, resembling the characteristics of a solid structure [27].

Figure 4 clearly demonstrates the presence of a plateau region in all lattice specimens of the CC-BCC type. The range of relative density Φ of 22-25% is a direct result of the lattice structure of CC-BCC. As the relative density Φ grows, the number of cavities that can cause the structure to collapse and produce the plateau region also increases. The investigation demonstrates the presence of buckling failure features, as depicted in **Figure 3**b. When exposed to strain, the CC-BCC specimen number 2 undergoes contraction in the central region of the structure.

The stress-strain graph of each lattice allows for the calculation of the experimental energy absorption per unit volume, Wc (MJ/m^3), experimental stiffness, $K_{0,c}$ (N/mm), and relative elastic modulus, E/Es. The experimental stiffness, $K_{0,c}$ is determined by calculating the slope or gradient in the elastic area using the Eq. (11).

$$K_{0,c} = \frac{dF}{dz}\bigg|\,(z = 0) \tag{11}$$

Where:

$K_{0,c}$: Experimental Stiffness, K0,c (N/mm)

dF : Force (N)

dz : Displacement (mm)

Meanwhile, the Relative Elastic Modulus is a ratio obtained by dividing the experimental modulus (E) by the material's elastic modulus (Es). The value of Es is 3500 MPa according to the PLA material properties table.

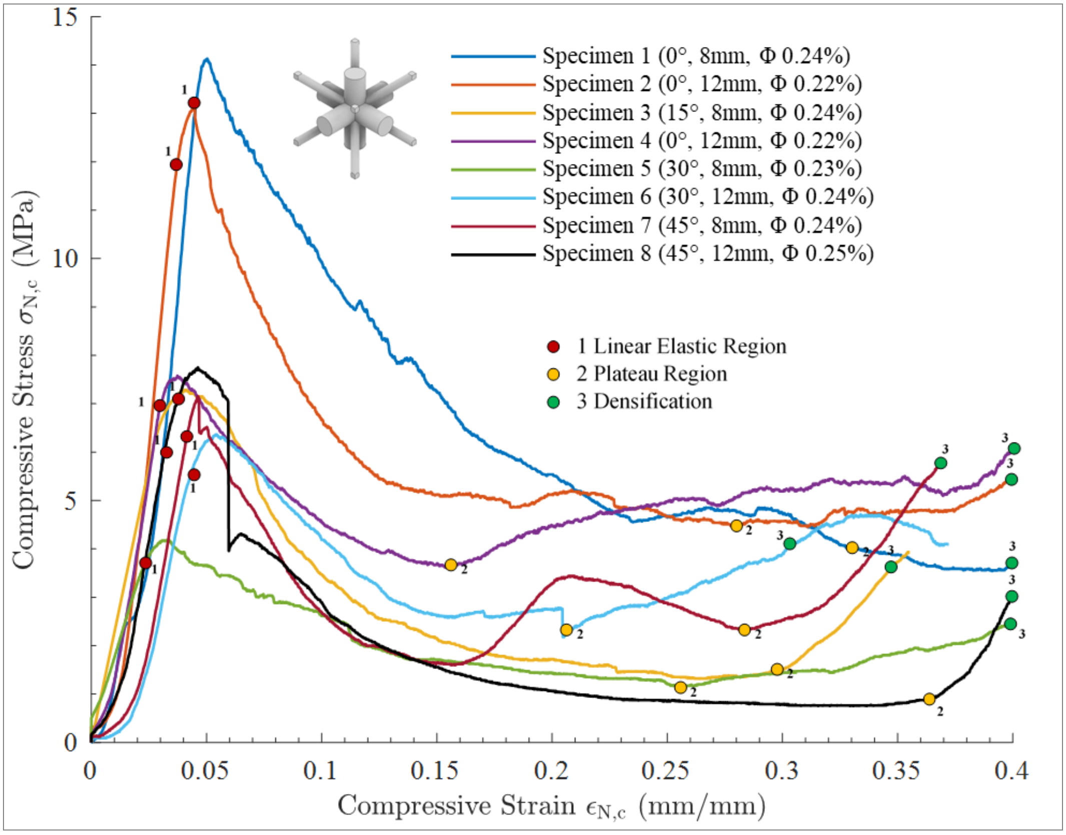

Figure 4. Experimental stress-strain curves of the compression tests on the lattice structures FDM Based CC-BCC

The lattice with a cell orientation of 0 degrees has compressive strength, energy absorption, stiffness, and relative elastic modulus values that are approximately 70-100% higher compared to other orientations (**Figure 5**(a-c)). This is certainly different from the isotropic nature that is expected to have the same mechanical properties in all directions [28]. Theoretical advancements unequivocally demonstrate that elastically-isotropic truss lattices in level material are still structurally anisotropic [29].

Finite Element Analysis (FEA) models and experimental data show comparable tendencies, as shown in **Figure 6**, with maximal compressive strength at 0°, a minimum at 30°, and a partial recovery at 45°. Larger diameter struts aligned perpendicular to the applied load give the structure a better strength at 0°, improving its resistance to normal loads and preventing buckling failures. In contrast to the 45° orientation, which, even with fewer struts, still aligns with the normal load, the lack of struts facing the usual direction at 15° and 30° causes bending and collapse failures, producing lesser strength. These outcomes align with the findings from Kumar et al. where they reported that small cells have higher stiffness and are more resistant to buckling [30]. T. You et al. also documented anisotropic behavior in lattices which are materially isotropic [31] during the analysis of different lattice orientations: [100], [110], and [111]. The compressive strength of the Octet Plate (OT-P) structure was found to be highest along the [100] direction, which aligns with our findings at the 0° lattice orientation. Our study is expected to complement previous research by introducing a more detailed range of orientations, using 15-degree increments from 0° to 45°.

In **Figure 7**, it shows maximum compressive Strength (MPa) in comparison with other standard cells for different orientation of cell. Lattice orientation had a significant effect on the compressive mechanical properties of the different structures and was based on the lattice type [32],[33]. Given the result of experimental and FEA Simulation, the CC-BCC Lattice did not distribute load evenly, therefore, CC-BCC lattice is structurally anisotropy [34]. Nevertheless, CC-BCC lattice in cell size of 8 mm has better performance at 0° and has quasi-isotropic strength in other orientation in comparison with octet cell that has contrast high strength at 45°. Meanwhile BCC cell has lowest strength in comparison with other lattices.

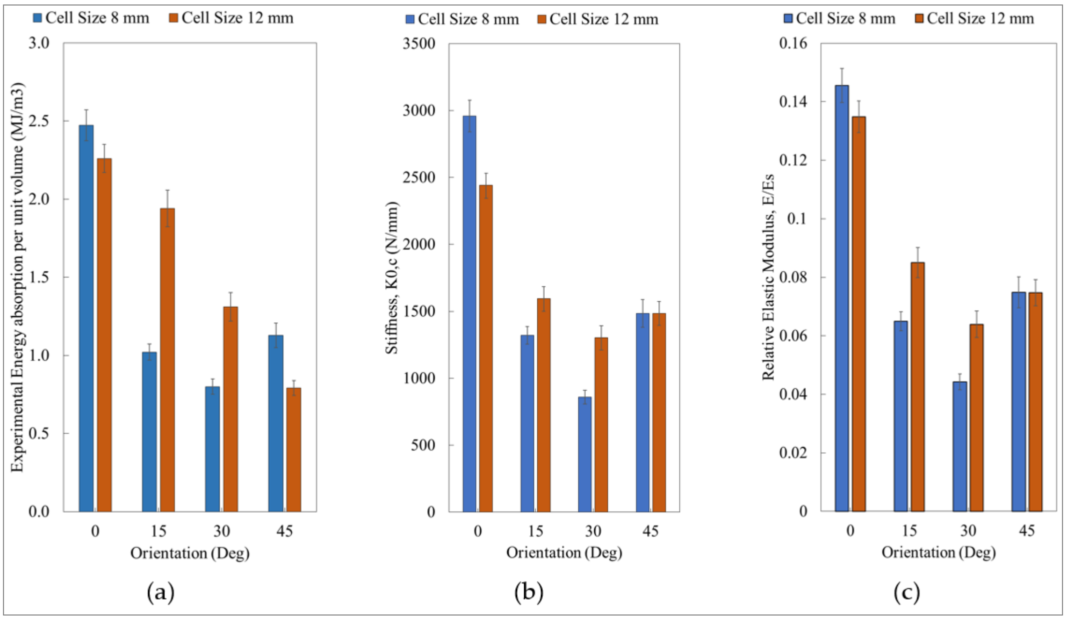

Figure 5. (a) Experimental Energy absorption per unit volume (MJ/m^3), (b) Stiffness, $K_{0,c}$ (N/mm), (c) Relative Elastic Modulus, E/Es

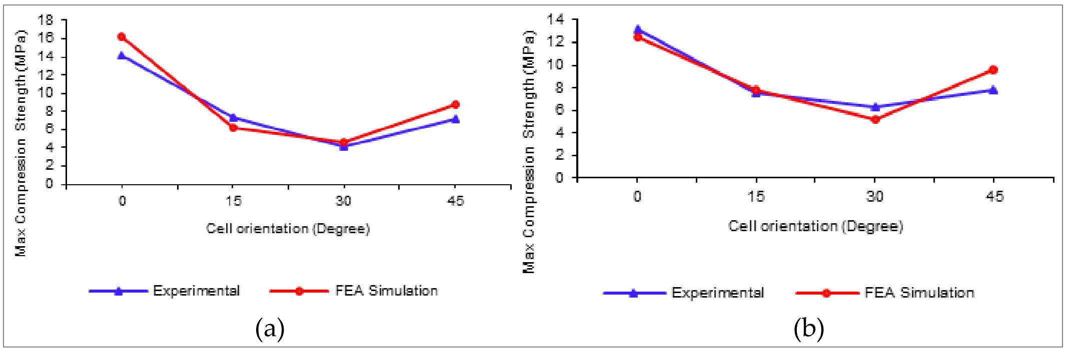

Figure 6. Maximum Compression Strength (MPa) Vs orientation with Cell Size (a) 3x3x3, (b) Cell Size 2x2x2

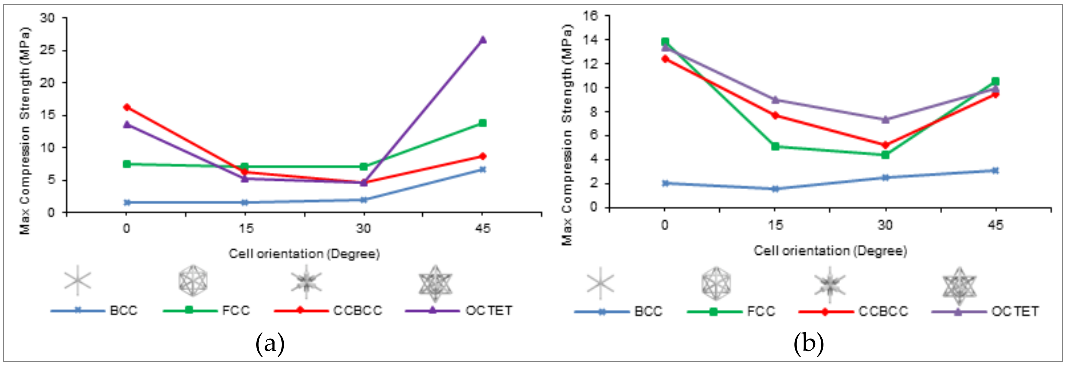

Figure 7. Maximum Compression Strength (MPa) Vs orientation in comparison with other standard cells (a) Cell Size 3x3x3, (b) Cell Size 2x2x2 (Φ is controlled within 22-25%)

The results of the FEA simulation shown in **Figure 8** explain that the stress obtained from the normal load will be directly transmitted by the CC strut facing the normal direction for 0° and 45° orientation [35]. This is different from the lattice with other cell orientations, where the stress will be distributed between the CC strut and the BCC strut for 15° and 30° orientation. In the context of a 0° orientation, the optimal mechanical properties were achieved with an 8 mm cell size. This results from its relative density of 0.24%, indicating that the lattice volume constitutes 24% of the cubic space volume. This aligns with previous studies indicating that relative density affects compressive strength [21]. The lattice with a 12 mm cell size at 15-45° orientations demonstrates superior mechanical capabilities relative to the 8 mm cell size. The relative density of the 12 mm cell is inferior to that of the 8 mm cell. This occurs because the lattice specimen shape is controlled within a cube, so when the cell is rotated, some spaces are fully filled while others are not. This is what causes the relative density characteristics at a 0° orientation to differ from those at other orientations.

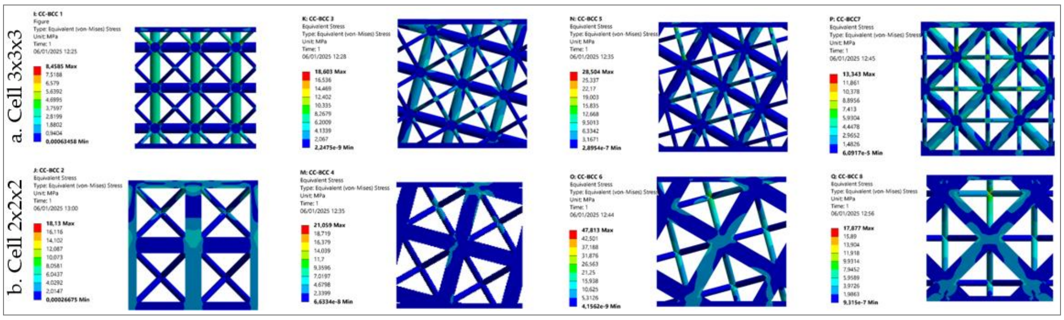

Figure 8. (a) Stress distribution with FEA Simulation with static load for Cell 3x3x3 (b) Stress distribution with FEA Simulation with static load for Cell 2x2x2

4. Conclusion

This research demonstrated the relationship between the isotropic properties of lattice structures at the material level and at the structural level, specifically tested the hypothesis that the combination of body-centered cubic (BCC) and crossing-cylinder(CC) lattices can create a new lattice structure with a CC/BCC strut diameter ratio of 2.5. This lattice cell has near-isotropic material properties with a Zener anisotropy index value of 1.08. These results indicated the importance of cell strut orientation at the structural level, as the potential strength of the lattice is aligned with the direction of the struts, achieving maximum strength when the strut direction is parallel to the applied force which proving that materially isotropic lattice is not always structurally isotropy. In addition to orientation, cell size also affects the compressive strength of the lattice structure, as compressive strength is influenced by the relative density of the lattice structure. To enhance the efficiency of isotropic lattice structures in various engineering applications, this research emphasized the need for a comprehensive approach in the design and optimization of additively manufactured components and encourages further investigation into the structural response of lattices.

Acknowledgments

The first author thankfully acknowledges the financial support provided by Indonesian Education Scholarship (BPI), Center for Higher Education Funding and Assessment (PPAPT), Ministry of Higher Education, Science, and Technology of Republic Indonesia (Kemdiktisaintek) and Indonesian Endowment Fund for Education (LPDP), Ministry of Finance of Republic Indonesia.

Authors' Declaration

Authors' contributions and responsibilities - The authors made substantial contributions to the conception and design of the study. The authors took responsibility for data analysis, interpretation, and discussion of results. The authors read and approved the final manuscript.

Funding – Indonesian Education Scholarship (BPI), Center for Higher Education Funding and Assessment (PPAPT), Ministry of Higher Education, Science, and Technology of Republic Indonesia (Kemdiktisaintek) and Indonesian Endowment Fund for Education (LPDP), Ministry of Finance of Republic Indonesia.

Availability of data and materials - All data is available from the authors.

Competing interests - The authors declare no competing interests.

Additional information – No additional information from the authors.

References

[1] M. Setiyo *et al.*, "Industry 4.0: Challenges of Mechanical Engineering for Society and Industry," *Mechanical Engineering for Society and Industry*, vol. 1, no. 1, pp. 3–5, 2021, doi: 10.31603/mesi.5309.

[2] G. P. Borikar, A. R. Patil, and S. B. Kolekar, *Additively Manufactured Lattice Structures and Materials: Present Progress and Future Scope*, vol. 24, no. 11. Korean Society for Precision Engineering, 2023. doi: 10.1007/s12541-023-00848-x.

[3] Y. Li, D. Jiang, R. Zhao, X. Wang, L. Wang, and L. C. Zhang, "High Mechanical Performance of Lattice Structures Fabricated by Additive Manufacturing," *Metals (Basel)*, vol. 14, no. 10, 2024, doi: 10.3390/met14101165.

[4] H. Gharehbaghi, A. Farrokhabadi, and Z. Noroozi, "Introducing a new hybrid surface strut-based lattice structure with enhanced energy absorption capacity," *Mechanics of Advanced Materials and Structures*, vol. 31, no. 14, pp. 2955–2964, 2024, doi: 10.1080/15376494.2023.2167246.

[5] A. Ahmad, L. Belluomo, M. Bici, and F. Campana, "Bird's Eye View on Lattice Structures: Design Issues and Applications for Best Practices in Mechanical Design," *Metals (Basel)*, vol. 13, no. 10, 2023, doi: 10.3390/met13101666.

[6] K. M. Park, K. S. Min, and Y. S. Roh, "Design Optimization of Lattice Structures under Compression: Study of Unit Cell Types and Cell Arrangements," *Materials*, vol. 15, no. 1, 2022, doi: 10.3390/ma15010097.

[7] Y. Lin *et al.*, "Influence of Density Gradient on the Compression of Functionally Graded BCC Lattice Structure," *Materials*, vol. 16, no. 2, 2023, doi: 10.3390/ma16020520.

[8] Z. Luo *et al.*, "Effect of aspect ratio on mechanical anisotropy of lattice structures," *Int J Mech Sci*, vol. 270, no. February, p. 109111, 2024, doi: 10.1016/j.ijmecsci.2024.109111.

[9] U. Hossain, S. Ghouse, K. Nai, and J. R. Jeffers, "Controlling and testing anisotropy in additively manufactured stochastic structures," *Addit Manuf*, vol. 39, no. January, p. 101849, 2021, doi: 10.1016/j.addma.2021.101849.

[10] X. Chen *et al.*, "A class of elastic isotropic plate lattice materials with near-isotropic yield stress," *Acta Mater*, vol. 276, no. June, p. 120085, 2024, doi: 10.1016/j.actamat.2024.120085.

[11] H. Yin and C. Liu, "Anisotropy and Asymmetry of the Elastic Tensor of Lattice Materials," *J Elast*, vol. 154, no. 5, pp. 659–691, 2023, doi: 10.1007/s10659-023-10028-7.

[12] D. Molavitabrizi and S. M. Mousavi, "Elasticity of Anisotropic Low-Density Lattice Materials," *Journal of Engineering Materials and Technology, Transactions of the ASME*, vol. 143, no. 2, 2021, doi: 10.1115/1.4048931.

[13] G. P. Steven, "Homogenization of multicomponent composite orthotropic materials using FEA," *Commun Numer Methods Eng*, vol. 13, no. 7, pp. 517–531, 1997.

[14] S. Daynes, "Isotropic cellular structure design strategies based on triply periodic minimal surfaces," *Addit Manuf*, vol. 81, no. January, p. 104010, 2024, doi: 10.1016/j.addma.2024.104010.

[15] S. Xu, J. Shen, S. Zhou, X. Huang, and Y. M. Xie, “Design of lattice structures with controlled anisotropy,” *Mater Des*, vol. 93, pp. 443–447, 2016, doi: 10.1016/j.matdes.2016.01.007.

[16] J. Feng, B. Liu, Z. Lin, and J. Fu, “Isotropic octet-truss lattice structure design and anisotropy control strategies for implant application,” *Mater Des*, vol. 203, p. 109595, 2021, doi: 10.1016/j.matdes.2021.109595.

[17] G. Dong, Y. Tang, and Y. F. Zhao, “A 149 Line Homogenization Code for Three-Dimensional Cellular Materials Written in MATLAB,” *Journal of Engineering Materials and Technology, Transactions of the ASME*, vol. 141, no. 1, pp. 1–11, 2019, doi: 10.1115/1.4040555.

[18] A. A. Arifin, I. M. L. Batan, M. Bici, A. Wahjudi, and A. S. Pramono, “Isotropic Body-Centered Cubic (BCC) Lattice Structure Design,” in *Smart Innovation in Mechanical Engineering*, A. El Kharbachi, I. D. Wijayanti, P. Suwarta, and I. Tolj, Eds., Singapore: Springer Nature Singapore, 2025, pp. 45–53.

[19] A. Kumar, L. Collini, A. Daurel, and J. Y. Jeng, “Design and additive manufacturing of closed cells from supportless lattice structure,” *Addit Manuf*, vol. 33, no. January, p. 101168, 2020, doi: 10.1016/j.addma.2020.101168.

[20] R. Ismail, M. A. Nursafitri, A. P. Fardinansyah, and D. Fajar, “Design , fabrication , and performance testing of an energy storage and return (ESAR) foot prosthesis made of prepreg carbon composite,” vol. 5, no. 1, 2025.

[21] Z. Fang, Y. Ding, Y. Jiang, Y. Zheng, Z. Wang, and F. Zhou, “Failure mode analysis of stiffness-guided lattice structures under quasi-static and dynamic compressions,” *Compos Struct*, vol. 275, no. July, p. 114414, 2021, doi: 10.1016/j.compstruct.2021.114414.

[22] Z. Wang, X. Jiang, G. Yang, B. Song, and H. Sha, “Design and mechanical performance analysis of T-BCC lattice structures,” *Journal of Materials Research and Technology*, vol. 32, no. June, pp. 1538–1551, 2024, doi: 10.1016/j.jmrt.2024.08.021.

[23] I. C. Scheperboer, A. S. J. Suiker, R. A. Luimes, E. Bosco, and A. J. M. Jorissen, “Collapse response of two-dimensional cellular solids by plasticity and cracking: application to wood,” *Int J Fract*, vol. 219, no. 2, pp. 221–244, 2019, doi: 10.1007/s10704-019-00392-8.

[24] N. Li, S. Pang, S. Chen, Y. Liu, W. Aiyiti, and Z. Chen, “Design and application of hybrid lattice metamaterial structures with high energy absorption and compressive resistance,” *Journal of Materials Research and Technology*, vol. 33, no. September, pp. 7100–7112, 2024, doi: 10.1016/j.jmrt.2024.11.113.

[25] L. Zhang *et al.*, “Energy absorption characteristics of metallic triply periodic minimal surface sheet structures under compressive loading,” *Addit Manuf*, vol. 23, no. July, pp. 505–515, 2018, doi: 10.1016/j.addma.2018.08.007.

[26] X. Ma, N. Zhang, Y. Chang, and X. Tian, “Multi-step deformation lattice structures from the rotation of unit cell,” *Int J Solids Struct*, vol. 288, no. November 2023, p. 112599, 2024, doi: 10.1016/j.ijsolstr.2023.112599.

[27] S. E. Alkhatib, A. Karrech, and T. B. Sercombe, “Isotropic energy absorption of topology optimized lattice structure,” *Thin-Walled Structures*, vol. 182, no. June 2022, p. 110220, 2023, doi: 10.1016/j.tws.2022.110220.

[28] S. Wang, Y. Zhu, J. Yu, L. Wang, and Z. Zheng, “Anisotropic mechanics of cell-elongated structures: Finite element study based on a 3D cellular model,” *Thin-Walled Structures*, vol. 205, no. PA, p. 112405, 2024, doi: 10.1016/j.tws.2024.112405.

[29] T. Tancogne-Dejean and D. Mohr, “Elastically-isotropic truss lattice materials of reduced plastic anisotropy,” *Int J Solids Struct*, vol. 138, pp. 24–39, 2018, doi: 10.1016/j.ijsolstr.2017.12.025.

[30] A. Kumar, L. Collini, A. Daurel, and J. Y. Jeng, “Design and additive manufacturing of closed cells from supportless lattice structure,” *Addit Manuf*, vol. 33, no. January, p. 101168, 2020, doi: 10.1016/j.addma.2020.101168.

[31] T. Yu *et al.*, “Truss and plate hybrid lattice structures: Simulation and experimental investigations of isotropy, large-strain deformation, and mechanisms,” *Mater Today Commun*, vol. 35, p. 106344, 2023, doi: https://doi.org/10.1016/j.mtcomm.2023.106344.

[32] K. Snodderly, A. Cunningham, N. Zipin, M. K. Sung, M. Di Prima, and D. Porter, “Effect of lattice orientation on compressive properties of selective laser sintered nylon lattice coupons,”

Mechanics of Materials, vol. 183, no. April, p. 104686, 2023, doi: 10.1016/j.mechmat.2023.104686.

[33] Y. Huang, A. R. O. Wan, K. Schmidt, P. Sefont, S. Singamneni, and Z. W. Chen, "Effects of cell orientation on compressive behaviour of electron beam powder bed fusion Ti6Al4V lattice structures," *Mater Today Proc*, no. xxxx, pp. 0–4, 2023, doi: 10.1016/j.matpr.2023.04.522.

[34] X. M. Delgado and C. G. Merrett, "Examination of isotropy assumption in isogrid structures through analysis and experimentation on four isogrid variations," *Acta Astronaut*, vol. 202, no. October 2022, pp. 422–432, 2023, doi: 10.1016/j.actaastro.2022.10.040.

[35] P. Li, F. Yang, Y. Bian, S. Zhang, and L. Wang, "Designable mechanical properties of modified body-centered cubic lattice materials," *Compos Struct*, vol. 317, no. April, 2023, doi: 10.1016/j.compstruct.2023.117060.